

the tuning efficiency is almost constant over the tuning range due to the nearly constant breakthrough voltage, which yields a heat generation proportional to the tuning current. The thermal wavelength shift roughly corresponds to a temperature increase of 40K indicating a thermal resistance of $\sim 120\text{K/W}$. As with the forward bias, the maximum wavelength shift is determined by the extinction of the laser operation. Under both biasing conditions the tuning behaviour is continuous, so that a total continuous tuning range of more than 11nm has been achieved, which exceeds the previously published data by more than 50%. The continuous tuning range of the as-cleaved devices has been found to be optimal for a laser length around $400\mu\text{m}$. This is because for the $200\mu\text{m}$ long devices the larger mirror losses reduce the margin for the threshold current raise, while in the $600\mu\text{m}$ long lasers the appearance of sidemodes during tuning limits the useful tuning range. By optimising the κL value and by using longer devices, therefore, a certain improvement in the tuning range appears still possible.

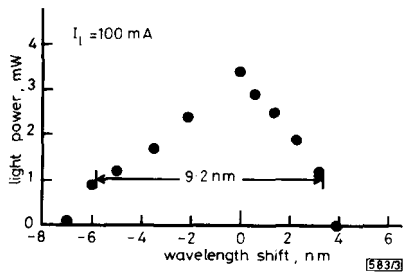


Fig. 3 Light power against wavelength shift of $400\mu\text{m}$ long TTG DFB laser with constant laser current of 100mA

The relationship between the light output power at one end facet ($NA = 0.5$) and the wavelength shift for the $400\mu\text{m}$ long lasers is plotted in Fig. 3. Starting with 3.5mW light power at zero tuning diode bias, the light power almost linearly drops with increasing wavelength shift for both the electronic and the thermal tuning mode. Thereby an optical power of more than 1mW can be maintained at a constant laser current of 100mA over a tuning

range of 9.2nm . Over this entire tuning range the SMSR remains above 40dB . By operating the tuning diode with a voltage controlled bias [12], i.e. applying a low impedance bias network, the injection recombination shot noise in the tuning region can be effectively suppressed so that the spectral linewidth is kept below 30MHz over this wavelength range. Furthermore the linewidth only slightly varies with tuning current, showing a monotonic increase from ~ 10 to 30MHz with an almost constant power-linewidth product by increasing the forward or backward biased tuning current.

In summary, we have presented an improved InGaAsP/InP TTG DFB laser structure for $1.5\mu\text{m}$ wavelength yielding a record continuous tuning range of 11nm . Over a wavelength range of 9.2nm an optical power of 1mW can be maintained with a spectral linewidth below 30MHz using $400\mu\text{m}$ long devices. No degradation of the tuning diode occurs under reverse bias, even at tuning currents up to 100mA , because the reverse current flows over the InP pn homojunctions outside the tuning region.

Acknowledgment: The authors gratefully acknowledge the technical assistance of V. Kulich, H. Michel, E. Noack, C. Raetzl and M. Schier. This work has been partly supported by the EC under RACE-project 2065 (COBRA).

© IEE 1993

27 September 1993

Electronics Letters Online No: 19931363

T. Wolf, S. Illek, J. Rieger, B. Borchert and M.-C. Amann (Siemens AG, Corporate Research and Development Otto-Hahn-Ring 6, 81730 Munich, Germany)

References

- 1 KOCH, T.L., and KOREN, U.: 'Semiconductor lasers for coherent optical fiber communications', *J. Lightwave Technol.*, 1990, **LT-8**, pp. 274-293

- 2 KOTAKI, Y. and ISHIKAWA, H.: 'Wavelength tunable DBF and DBR lasers for coherent optical fibre communications', *IEE Proc. J.*, 1991, **138**, pp. 171-177
- 3 WOODWARD, S.L., PARAYANTHAL, P., and KOREN, U.: 'The effects of aging on the Bragg section of a DBR laser', *IEEE Photonics Technol. Lett.*, 1993, **5**, pp. 750-752
- 4 EBBERG, A., and NOÉ, R.: 'Novel high precision alignment technique for polarisation maintaining fibres using a frequency modulated tunable laser', *Electron. Lett.*, 1990, **26**, pp. 2009-2011
- 5 SCHELL, M., HUHSE, D., and BIMBERG, D.: 'Generation of short (3.5 ps) low jitter (<math><100\text{fs}</math>) light pulses with a $1.55\mu\text{m}$ tunable twin guide laser'. Tech. Dig. 19th European Conf. on Optical Communications, 1993, (Montreaux, Switzerland), pp. 229-232
- 6 HEYDT, G., KHOE, G.D., RAGDALE, C., and EBBERG, A.: 'RACE project R1010 scenario for the implementation of coherent multichannel systems in the subscriber area of the European IBC network', *Opt. & Quantum Electron.*, 1990, **22**, pp. 535-554
- 7 NOÉ, R., DRÖGEMÜLLER, K., RODLER, H., EBBERG, A., MEIBNER, E., BODLAJ, V., WITTMAN, J., AURACHER, F., BORCHERT, B., WOLF, T., AMANN, M.-C., BAUER, J., ALBRECHT, K., PAZELT, K., and ALTHAUS, H.I.: 'Fully engineered coherent multichannel transmitters and receivers using data-induced polarization switching'. Tech. Dig. Optical Fiber Conf., 1992, (San Jose, USA), p. 286
- 8 ILLEK, S., THULKE, W., SCHANEN, C., LANG, H., and AMANN, M.-C.: 'Over 7nm (875GHz) continuous wavelength tuning by tunable twin-guide (TTG) laser diode'. *Electron. Lett.*, 1990, **26**, pp. 46-47
- 9 KUINDERSMA, P.I., DCHEEPERS, W., CNOOPS, J.M.H., THUIS, P.J.A., V.D. HOFSTAD, G.L.A., DONGEN, T.V., and BINSMA, J.J.M.: 'Tunable three-section, strained MQW, PA-DFB's with large single mode tuning range (72Å) and narrow linewidth (around 1MHz)'. Conf. Dig. 12th IEEE Semiconductor Laser Conf., 1990, (Davos, Switzerland), pp. 248-249
- 10 TOHYAMA, M., ONOMURA, M., FUNEMITSU, M., and SUZUKI, N.: 'Wavelength tuning mechanism in three-electrode DFB lasers', *IEEE Photonics Technol. Lett.*, 1993, **5**, pp. 616-618
- 11 OEBERG, M., NILSSON, S., KLINGA, T., and OJALA, P.: 'A three-electrode distributed Bragg reflector laser with 22nm wavelength tuning range', *IEEE Photonics Technol. Lett.*, 1991, **3**, pp. 299-301
- 12 STEGEMÜLLER, B., VEUHOFF, E., RIEGER, J., and HEDRICH, H.: 'High-temperature (130°C) CW operation of $1.53\mu\text{m}$ InGaAsP ridge-waveguide lasers using strained quaternary quantum wells', *Electron. Lett.*, 1993, **29**, (19), pp. 1691-1693
- 13 AMANN, M.-C., ILLEK, S., and LANG, H.: 'Linewidth reduction in wavelength tunable laser diodes by voltage control', *Electron. Lett.*, 1991, **27**, pp. 531-532

Polarisation-rotating quasioptical reflection amplifier cell

H.S. Tsai and R.A. York

Indexing Terms: Antennas, Microstrip, Amplifiers

A quasioptical amplifier cell suitable for power-combining arrays is presented. Orthogonally polarised patch antennas are coupled to the input and output of a resistive-feedback MESFET amplifier. A simple polarimetric reflectometer was developed to test the amplifier cell which solves the problem of imperfect isolation between transmitting and receiving horns and the DC offset problem of quadrature detectors. A peak effective isotropic power gain (EIPG) of 17dB was measured at 4.2GHz with 1% bandwidth which is limited by patch antennas.

Introduction: Solid-state power combining in free space offers an attractive alternative to vacuum-tube sources for high power millimetre wave applications [1]. Quasioptical oscillator arrays have been developed to prove this concept [2]. More recently, attention has been focused on developing high-power quasioptical amplifier arrays, and a grid amplifier array and single-element amplifier have been demonstrated [3,4]. Both of these are transmission-type amplifiers, where signals incident on one side of the substrate are received, amplified, and retransmitted through the opposite side in an orthogonal polarisation. In this Letter, a reflection-type planar amplifier is presented using orthogonally polarised patch antennas and a resistive feedback single-stage amplifier. Reflection amplifiers are attractive because they are compact, and the signals do not

propagate through the substrate so the backside can be used for waste heat removal, which will be critical in high-power, high-efficiency designs.

Amplifier and matching network design. Because this work is aimed at future monolithic arrays, our designs were fabricated on a high dielectric constant substrate which closely approximates that of GaAs. The actual substrate material was Rogers Duroid 6010 with a dielectric constant of 10.8 and thickness of 25mil (0.635mm). A resistive feedback amplifier design was chosen [5], using a packaged GaAs MESFET (NE32184A). The design frequency was 4GHz and the input and output patch antennas were orthogonally polarised.

From the manufacturer's data sheet, the transconductance of this MESFET, g_m , is typically 33 mS. Let A be voltage gain of this amplifier, R_f be the feedback resistor and Z_o be the source and load impedance. Use of design equations [5]

$$R_f = Z_o(1 - A) \quad g_m = \frac{1 - A}{Z_o} \quad (1)$$

will lead to

$$Z_{in} = Z_{out} = Z_o \quad (2)$$

where Z_{in} and Z_{out} are defined as the input and output impedances of this amplifier. If R_f is chosen to be 511Ω (a value of chip resistor available in our laboratory), the voltage gain A will be -3.1 which corresponds to -10dB power gain and Z_o will be 125Ω

The design is complicated by the fact that the source and load impedances are complex (patch antennas). The patch antenna can be modelled as a half wavelength transmission line with a radiation resistance at both ends [6]. At resonance the input impedance is real and given by the parallel combination of the two radiation resistances. Double radial stubs were used in the matching network to transform the impedance (at resonance) to 125Ω. The whole circuit including the patch antennas, matching networks and amplifier, was simulated with the CAD package Libra [Note 1] to obtain a good match at resonance; this was done by modifying the internal terminating impedance of the simulator from 50 to 995Ω, the value of radiation resistance for our design [6]. The actual layout of the amplifier is shown in Fig. 1. The two source leads were soldered to the ground plane through the substrate. The feedback resistor was soldered 'piggy-back' on top of the transistor between gate and drain. DC bias was applied through high impedance lines connected to the middle of the patch antennas, which is a low impedance point. Bypass capacitors were used to avoid oscillation at low frequencies.

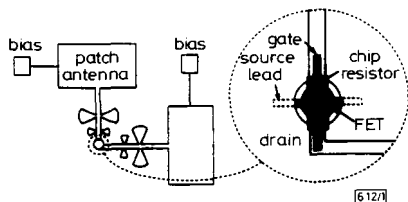


Fig. 1 Plan view of patch-coupled amplifier circuit, with blow-up of resistive feedback amplifier

The source leads are soldered to the ground plane through the substrate

Measured Results: The amplifier was measured in the far-field using the setup shown in Fig. 2, which is essentially a CW homodyne radar system with separate, orthogonally polarised transmit and receive antennas (waveguide horns). By modulating the bias to the antenna and using a lock-in detector to sample the quadrature mixer outputs (here used as a phase detector), the imperfect isolation between the horn antennas can be overcome, with an added benefit of eliminating the problem of DC offset in the quadrature mixer [7]. The system is calibrated by replacing the amplifier with a standard gain horn which radiates a known power. The effective isotropic power gain (EIPG) of this amplifier cell, which is the quantity that is actually measured, is given by [5]

Note 1: Libra is a registered trademark of EEsof, Inc., Westlake, CA.

$$EIPG = G_p^2 G_A = \left[\frac{V_{ra}}{V_{rc}} \right]^2 \frac{P_{cali}}{P_{tran}} \left[\frac{4\pi R^2}{\lambda} \right]^2 \frac{G_2}{G_1} \quad (3)$$

where G_A and G_p are the gains of amplifier and patch antenna, respectively. V_{rc} and V_{ra} are the voltages recorded by a lock-in amplifier during calibration and actual measurement. P_{cali} is the power transmitted during calibration by the standard gain horn with a gain of G_2 , and P_{tran} is the power transmitted during the measurement through a horn with a gain of G_1 . λ is the free-space wavelength and R is the distance between the receiver and the amplifier.

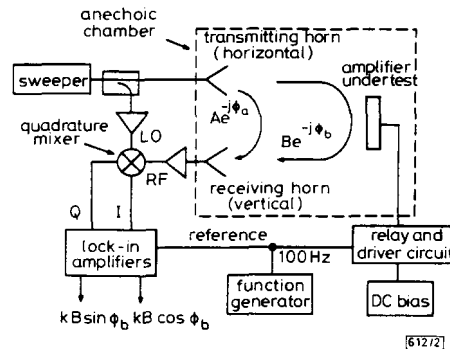


Fig. 2 Illustration of free-space reflection measurement setup

The array bias is modulated and the received signal detected using a quadrature receiver and lock-in amplifier

Assuming a typical patch antenna gain G_p of 5dB, the amplifier gain can be extracted from eqn. 3 and is shown in Fig. 3. The peak gain is ~7dB with 1% bandwidth. The low gain could be a result of an impedance mismatch, a lower g_m than expected, and also a different patch gain than the assumed 5dB. Also shown in Fig. 3 is the expected frequency response of both input and output patch antennas (shifted upwards on the graph by 7dB to match the gain curve) which indicates that the bandwidth of this amplifier is limited by patch antennas, not by the amplifier. The curve for reverse gain in the Figure was measured by rotating the amplifier 90° along the propagation axis, and is at least 25dB lower than the forward gain over the frequency band, indicating that the free-space amplifier is polarisation selective.

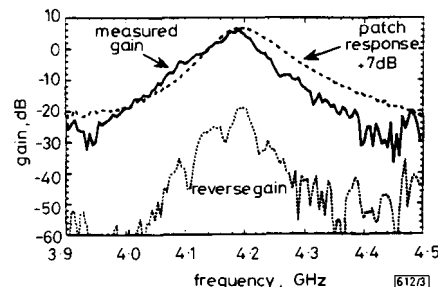


Fig. 3 Measured forward and reverse power gain of amplifier cell assuming a patch gain of 5dB, and comparison with frequency response of patch antennas

Conclusion: A reflection-type free-space amplifier and measurement technique have been developed, giving a measured gain of ~7dB with 1% bandwidth. The bandwidth of this amplifier is limited by the resonant patch antennas on a thin substrate with high dielectric constant. The future work will focus on increasing bandwidth by either modifying the patch antennas or using other broadband antennas, such as the bow-tie and folded slot antennas.

Acknowledgment: This work was supported by the Rockwell Science Center in Thousand Oaks, California.

References

- 1 MINK, J.W.: 'Quasi-optical power-combining of solid-state millimeter-wave sources', *IEEE Trans.*, February 1986, **MTT-34**, pp. 273-279
- 2 YORK, R.A., and COMPTON, R.C.: 'Quasi-optical power-combining using mutually synchronized oscillator arrays', *IEEE Trans.*, June 1991, **MTT-39**, pp. 1000-1009
- 3 KIM, M., ROSENBERG, J.J., SMITH, R.P., WEIKLE II, R.M., HACKER, J.B., DELISIO, M.P., and RUTLEDGE, D.B.: 'A grid amplifier', *IEEE Microw. & Guided Wave Lett.*, 1991, **1**, (11), pp. 322-324
- 4 CHI, C.Y., and REBEIZ, G.M.: 'A quasi-optical amplifier', *IEEE Microw. & Guided Wave Lett.*, 1993, **3**, (6)
- 5 VENDELIN, G.D., PAVIO, A.M., and ROHDE, U.L.: 'Microwave circuit design' (John Wiley & Sons, 1990)
- 6 JAMES, J.R., HALL, P.S., and WOOD, C.: 'Microstrip antenna - Theory and design' (Peter Peregrinus Ltd., 1981)
- 7 TSAI, H.S., KENT, D., LEE, H., and YORK, R.A.: 'Far-field reflectometry for characterization of active antennas', submitted to *IEEE Trans. Instrumentation Meas.*, 1993

Efficient calculation of surface impedance for rectangular conductors

E. Tuncer and D.P. Neikirk

Indexing terms: Skin effect, Numerical methods

The Letter presents a new expression for the frequency-dependent surface impedance of a rectangular bar that is easily used, and is numerically efficient. By dividing the metal bar into rectangular and square sections, skin depth-induced current crowding to the surfaces and corners can be accurately modelled. Comparison with measured data shows excellent agreement over a wide frequency range, covering the transition from DC-like behaviour to skin-depth limited behaviour.

Introduction: Recently a new, simple technique for the evaluation of conductor loss in quasi-TEM transmission lines has been demonstrated [1, 2]. Efficient use of this conformal mapping technique requires knowledge of the specific surface impedance of each conductor in the transmission line. For a conductor with circular cross-section, it is possible to solve the Helmholtz equation exactly. However, many transmission lines make use of conductors with rectangular cross-section. There are a variety of techniques that have been developed for use with rectangular cross-sections, but many are numerically intensive. In this Letter we show a new, numerically efficient technique that accurately predicts the surface impedance of rectangular bars ranging in aspect ratio from a square bar to a wide flat plate.

Model: A very simple approximation for the specific surface impedance Z_s (in Ω/\square) of a flat conductor that is much wider than it is thick (i.e. a thin conducting plate) is [3]

$$Z_s^{\text{plate}} = \frac{\sqrt{\frac{\omega\mu}{\sigma}}(1+j)}{\tanh\left\{\sqrt{\frac{\omega\mu\sigma}{2}}\left(\frac{t}{\delta}\right)(1+j)\right\}} \quad (1)$$

$$= \frac{\frac{1}{\sigma\delta}(1+j)}{\tanh\left\{\frac{1}{2}\left(\frac{t}{\delta}\right)(1+j)\right\}}$$

where t is the thickness and σ is the conductivity of the conductor, ω is the angular frequency, μ is the permeability of the metal, and δ is the skin depth in the conductor. Note that because the plate has two surfaces, eqn. 1 must be used for each side of the conductor. In time domain simulations it is quite important that the surface impedance have the correct DC behaviour. The appropriate DC limit of eqn. 1 should be $2R_s$ (the factor of 2 appearing because this resistance represents only one side of the plate), where R_s is the DC sheet resistance of the entire plate (given by $1/\sigma t$). It

is easily verified that eqn. 1 does produce the appropriate low frequency limit, i.e. as $\omega \rightarrow 0$, $Z_s \rightarrow 2/\sigma t$

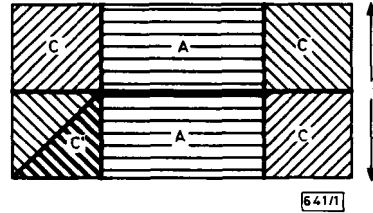


Fig. 1 Thick rectangular conductor

The surface impedance of regions A is given approximately by eqn. 1, and region C by eqn. 5

For rectangular conductors with appreciable thickness, however, the simple result given by eqn. 1 will not hold. An accurate approximate expression for a thick conducting plate should yield both the correct DC resistance of the conductor as $\omega \rightarrow 0$ as well as the proper skin effect behaviour at high frequency. The simplest approach is to divide the rectangular cross-section into segments, as shown in Fig. 1. Note that the frequency dependence is set by the ratio of the skin depth to the thickness of the conducting region. For the rectangular regions (segments A in Fig. 1) this is just half the thickness t , so the rectangular sections should have a surface impedance given by eqn. 1.

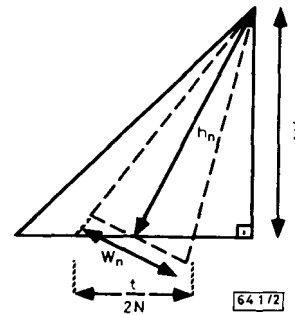


Fig. 2 n th triangular patch in corner region C' of Fig. 1

The triangular transmission line used for input impedance calculation has length h_n and width w_n .

In the square corner sections (segments C in Fig. 1) the skin effect will cause current crowding toward the outside corner of the region. By symmetry, we need only find the surface impedance of half of the square region, divided along a diagonal (region C' in Fig. 1). To capture this effect, consider Fig. 2 for region C' of the conductor. We divide the region into N triangular patches, and use the distance from the base of each patch to the inside corner, h_n , as the thickness of this segment of conductor. For the n th ($n = 0, 1, 2, \dots, N-1$) segment in Fig. 2, the height h_n is given by

$$h_n = \frac{t}{2} \sqrt{1 + \left(\frac{n + \frac{1}{2}}{N}\right)^2} \quad (2)$$

and the width w_n by

$$w_n = \frac{h_n}{2} \left[\frac{1}{N + (n + \frac{1}{2})\frac{n}{N}} + \frac{1}{N + (n + \frac{1}{2})\frac{n+1}{N}} \right] \quad (3)$$

For a triangular section, the surface impedance expression can be found by applying transverse resonance and non-uniform transmission line analysis [4, 5]. The total input impedance for a triangular transmission line with width w_n (at the input end, or front surface), plate separation of one unit distance, and length h_n , filled with a uniform conducting material of conductivity σ , assuming an open circuit termination, is

$$Z_{in} = j \sqrt{\frac{j\omega\mu\sigma}{w_n\sigma}} \frac{J_0(j\sqrt{j\omega\mu\sigma}h_n)}{J_1(j\sqrt{j\omega\mu\sigma}h_n)} \quad (4)$$

where J_0 and J_1 are Bessel functions of the first kind. The